Development of a statistical dynamic radiation belt model: Analysis of storm time particle flux variations

Mazzino, Laura; Cyamukungu, Mathias; Benck, Sylvie; Cabrera, Juan

Center for Space Radiations, Chemin du Cyclotron, 2 B-1348 Louvain-la-Neuve, Belgium
32 (0)10 47 34 02 (mazzino@spaceradiations.be)

ABSTRACT

Magnetic storms and their subsequent energetic particle flux enhancements constitute an important issue dealt with in space weather studies. These flux variations significantly contribute to the increased variances that spoil statistical ionizing radiation flux models, i.e., results of flux measurements at a given position in space can only be accurately predicted if the past geomagnetic activity is well specified. Therefore, the RABEM/SEVEM particle and wave dynamical model is based on the assumption that the particle fluxes and wave intensities at a given position in space are composed of a steady state background and a magnetic activity-dependent value that is a function of the elapsed time after the latest geomagnetic storm (GS), the intensity of the latest GS, the flux level prior to the latest GS, the local flux decay time and the occurrence probability for a new GS. Fifty years of GS events characterized by their minimum Dst have been analyzed and the statistical distribution of time intervals between GS along with their magnitude was derived at several times within the solar cycle. Flux data from different sources are analyzed to establish a relationship between flux enhancement and storm characteristics. In particular, using the DEMETER and the SAC-C flux data, we have identified GS events in 2001-2005, where the magnitude of the maximum flux enhancement goes in hand with the magnitude of the storms, for electrons between 0.521 and 0.968 MeV for $L > 2.5$ and $B > 0.22$ nT. In addition, decay times of fluxes have been evaluated as a function of energy and position. The steps accomplished during the ongoing RABEM/SEVEM model development activity will be described and preliminary results of the study will be presented.

1. INTRODUCTION

Energetic particle flux enhancements produced by magnetic storms constitute an important issue in space weather studies. The current accepted models AE8 and AP8 have been successfully used to predict average fluxes for decades at high altitude. The flux maps in [L-value, B/B_o] coordinates for different energies used to develop these models are based on data from more than 20 satellites flown during the early sixties until the mid-seventies. However, some of the problems with both models are that they display huge discrepancies with recent data acquired at low altitudes, that magnetic storm effects are not yet included in any of the AE maps and that none of the flux maps consider time variations beyond the solar cycle minimum and maximum distinction [Xapsos et al, 2002][1], [Gussenhoven et al, 1996] [2]. Therefore, the RABEM/SEVEM particle and wave dynamical model (RABEM=Radiation Belt Models; SEVEM = Statistical ELF and VLF Environment Models) has as primary goal to resolve some of these problems. This model is based on the study of radiation belt flux response during storm times, wave-particle interaction, and includes a mapping for all regions and energy ranges.

The preliminary studies presented in this paper, a definition of a statistical dynamic radiation belt model, will serve to find the appropriate parameters for the model, as well as to help radiation belt (RB) theoreticians validate processes which involve wave-particle interactions. In addition, engineers that are concerned about damage to satellites may benefit from these studies by being able to predict hazardous events in the space radiation environment.

2. BASIS OF THE RABEM/SEVEM STATISTICAL DYNAMIC RADIATION BELT MODEL

In 1966 McIlwain identified five processes that explained well the time dependence behavior of electron fluxes, measured in Explorer XV[McIlwain, 1996][3]. These processes are: Rapid non-adiabatic acceleration (produced during the recovery phase of magnetic storms), persistent decay (pitch angle scattering of electrons into the loss cone after the storm), radial diffusion, adiabatic acceleration (it seems to occur when magnetic field is distended by ring current particles/ring current magnetic fields cause an adiabatic acceleration of inner zone protons), and rapid loss (that could be in energy or number of particles, dropped by opening tail). Combining these five processes, McIlwain was able to produce a curve of the energetic electron storm measured in Explorer XV.

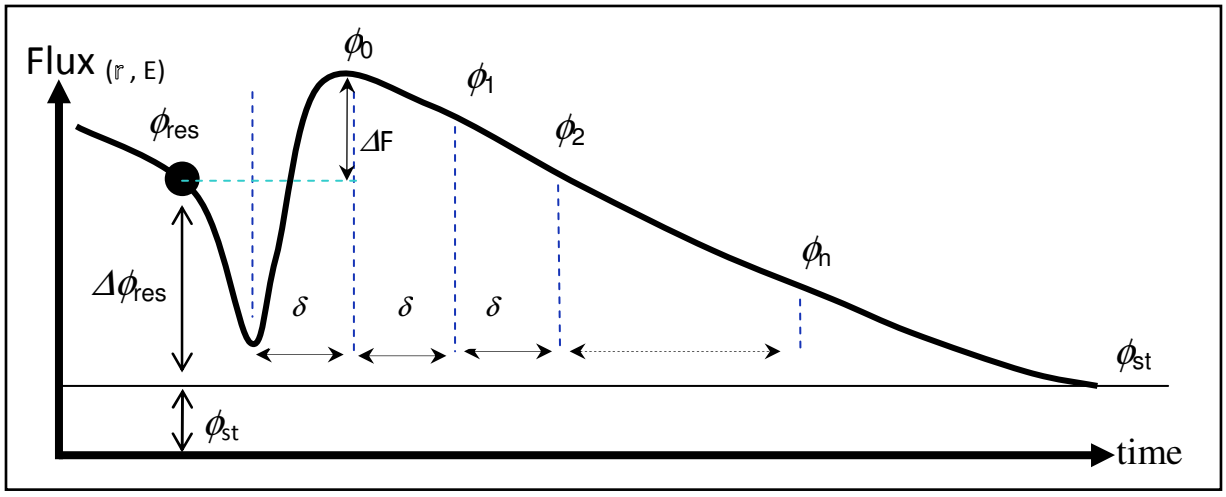

Figure 1: Flux enhancement for storm-time as a function of time. After a GS, there is a rapid non-adiabatic acceleration, until the maximum flux ϕ_0 is reached, starting the persistent decay.

In the RABEM/SEVEM statistical dynamic model presented in this paper, these five processes were used to develop a storm-time model for the RB.

3. THE RABEM/SEVEM STATISTICAL DYNAMIC RADIATION BELT MODEL

Storm time flux variations significantly contribute to the increased variances that spoil statistical ionizing radiation flux models, i.e., results of flux measurements at a given position in space can only be accurately predicted if the past geomagnetic activity is well specified. Therefore, the RABEM/SEVEM statistical dynamic radiation belt model is based on the assumption that the particle fluxes at a given position in space are composed of a steady state background and a magnetic activity-dependent value that is a function of the elapsed time after the latest geomagnetic storm, the intensity of the latest GS, the flux level prior to the latest GS, the local flux decay time and the occurrence probability for a new GS.

Consider the flux enhancement during storm-time (Figure 1) for a given position and energy range. Before a GS, or sometimes during the main phase of the storm, the flux continues decaying from the previous storm to reach certain value, which will be called 'flux residual' ϕ_{res}, which does not include any response of this new GS. After Dst reaches a minimum value (Dst_{prev}), initiating the recovery phase of the storm, the rapid non-adiabatic acceleration (McIlwain process 1) is observed.

For certain high energy ranges, there is a drop out just before this process; in Figure 1 there is an assumption that the drop out minimum is at about the same time of Dst minimum (Dst_{prev}). The non-adiabatic acceleration continues during the recovery phase of the storm, until the flux enhancement reaches a maximum, called ϕ_0, by the end of the GS, which indicates the commencement of the persistent decay (McIlwain process 2), due to pitch angle scattering of electrons into the loss cone after the GS. The maximum flux reached can be expressed as:

$$\phi_0 = \phi_{st} + \Delta\phi_{res} + \Delta F(Dst_{prev}) \quad (1)$$

where ϕ_{st} is the steady state flux measured during quiet times for that particular position and energy range, $\Delta\phi_{res}$ is the difference between flux before storm and steady state flux, Dst_{prev} is the minimum value reached by Dst in the GS, and $\Delta F(Dst_{prev})$ is the flux variation induced by previous storm of minimum Dst_{prev}. The time after the persistent decay has begun can be divided into equal time segments to provide time slots for prediction of electron fluxes; for convenience the time segments will be equal to δ, time elapsed from the storm minimum Dst_{prev} (or drop-out min) to ϕ_0. For any later time, $n\delta$, the flux can be predicted as:

$$\phi_n = \phi_{st} + (\phi_{n-1} - \phi_{st})\, e^{-\delta/T} + \Delta\phi_n \quad (2)$$

where T is the decay time of flux at a given space position for a given energy, and $\Delta\phi_n$ is the flux variation following a storm (average) due to the probability $P(Dst_k)$ of having a GS with Dst_k value during the considered time interval. This $\Delta\phi_n$ can be obtained, as shown in Eq. 3 from the Dst probabilities, given the number of bins in Dst_k range N and its subsequently flux enhancement difference associated $\Delta F(Dst_k)$.

$$\Delta\phi_n = \sum_{k=0}^{N} P(Dst_k \mid n\delta, Dst_{prev}, type, s) \times (\Delta F(Dst_k)) \quad (3)$$

The variance on $\Delta\phi_n$ can be calculated as:

$$\sigma_{\Delta\phi_n} = \sqrt{\sum_{k=0}^{N_{act}} P(Dst_k \mid n\delta, Dst_{prev}, solar, type) \times (\Delta F(Dst_k) - \overline{\Delta F}(Dst))^2} \quad (4)$$

In the following section, the parameters ($\Delta\phi_{res}$, ϕ_0, ϕ_{st}, T,…) that need to be considered in order to evaluate ϕ_n (Eq. 2) are investigated, including the flux response and the probability of having a GS given the characteristics of the previous GS. For example, a variation of the *type* of storm, such as Coronal Mass Ejections (CMEs), Corotating Interaction Regions (CIRs) or multiple storm that includes both types, would result in a difference on the recovery time interval, and therefore, the time between GS and maximum flux ϕ_0, as well as the magnitude of ϕ_0 [Kataoka and Miyoshi, 2006][4] . Differences in frequency of GS occurrence for solar cycles more active than others have been observed. Moreover, those differences extend to phases (min, increasing, max, decline) within the same solar cycle, and indicate that a solar activity index parameter *s*, such as sunspot number or the F10.7cm index, needs to be considered as well.

4. DERIVATION OF PARAMETERS AND STATISTICS

Fifty years of GS events characterized by their minimum Dst have been analyzed. The data set was downloaded from the World Data Center for Geomagnetism (WDC).[5] GS were identified when their Dst values were less than –50 nT. All substorms, defined as magnetic storms with Dst values greater than –50 nT, were not considered in the analysis.

Important preliminary results:

i. The probability of a given storm amplitude depends on the amplitude of the previous storm. The probability of having a storm following another decreases as the value of Dst decreases. If the GS previous had a higher value of Dst, the probability of having a storm of any intensity is higher than if the previous storm had a lower value (Fig. 2)
ii. The storm occurrence appears to be a poissonnian process when amplitude is not taken into account. (Fig. 3)
iii. Most events (90%) can be identified by $Dst_k > -190$ nT, and time interval between storms less than 50 days. (Fig. 4).
iv. The distribution of GS as a function of time for the period analyzed (from1957 to 2007) clearly shows a dependence between solar cycle characteristics and GS occurrences, represented in Fig. 5 with sunspot number (SSN) [6]. The total number of storms in a cycle correlates directly to the severity of the solar cycle (SC): for solar cycles with higher SSN maxima, SC 21 and SC 22, the total number of storms is higher than for SC 20 and SC 23 with lower maxima, even though their duration time in both cases is significantly longer than for SC 21 and SC 22. Notice that, given the fact that the Dst data of the SC 19 is not complete, it was not considered in the statistical analysis.

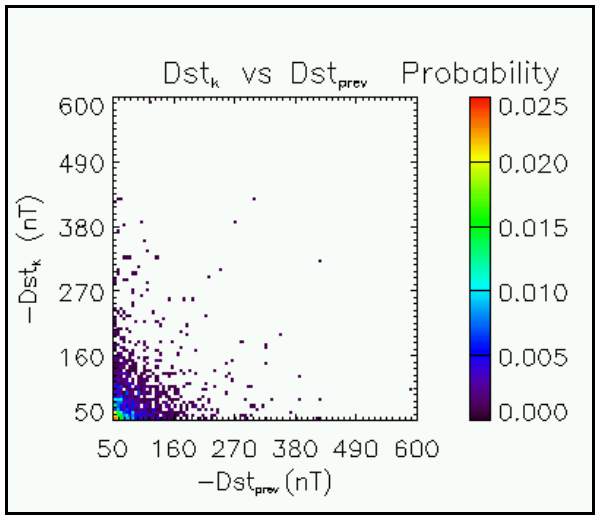

Figure 2 (a) Histogram of absolute Dst_k vs. Dst_{prev}, number of bins = 100. The probability of having a storm following another decreases as the value of Dst decreases (vertical direction) and increases if Dst_{prev} has a higher value (horizontal direction).

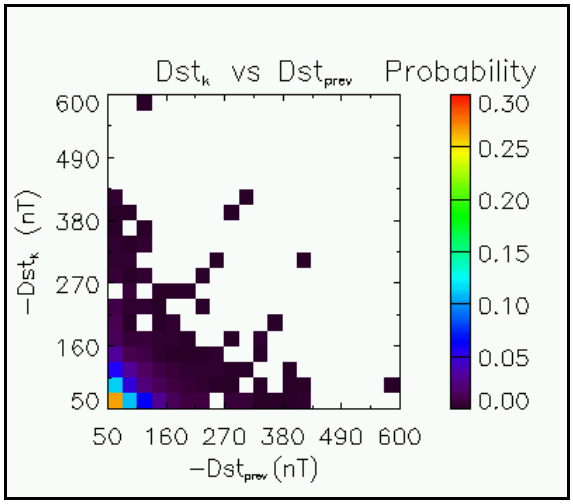

Figure 2 (b) Histogram of absolute Dst_k vs. Dst_{prev}, number of bins = 20

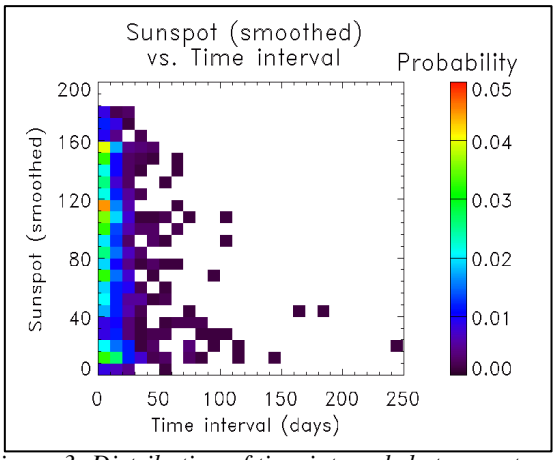

Figure 3: Distribution of time intervals between storms with Dst < -50 nT, for various Sunspot number values. The geomagnetic storm occurrence appears to be a poissonnian process when amplitude is not taken into account.

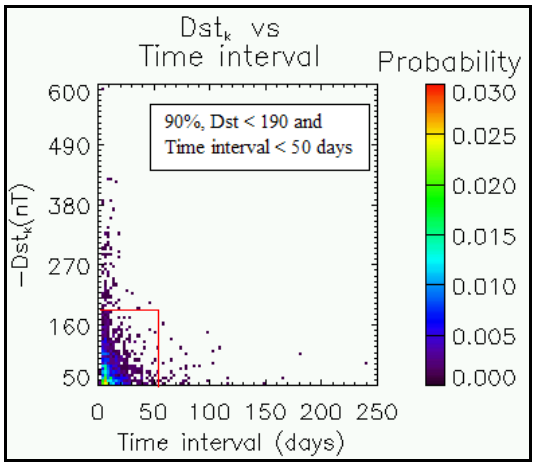

Figure 4: Histogram of Dst_k vs. time interval (between Dst_k and Dst_{prev}). For few events the time interval between storms is greater than 100 days, and the time interval between those storms can be used to find the steady state as shown in section 5.

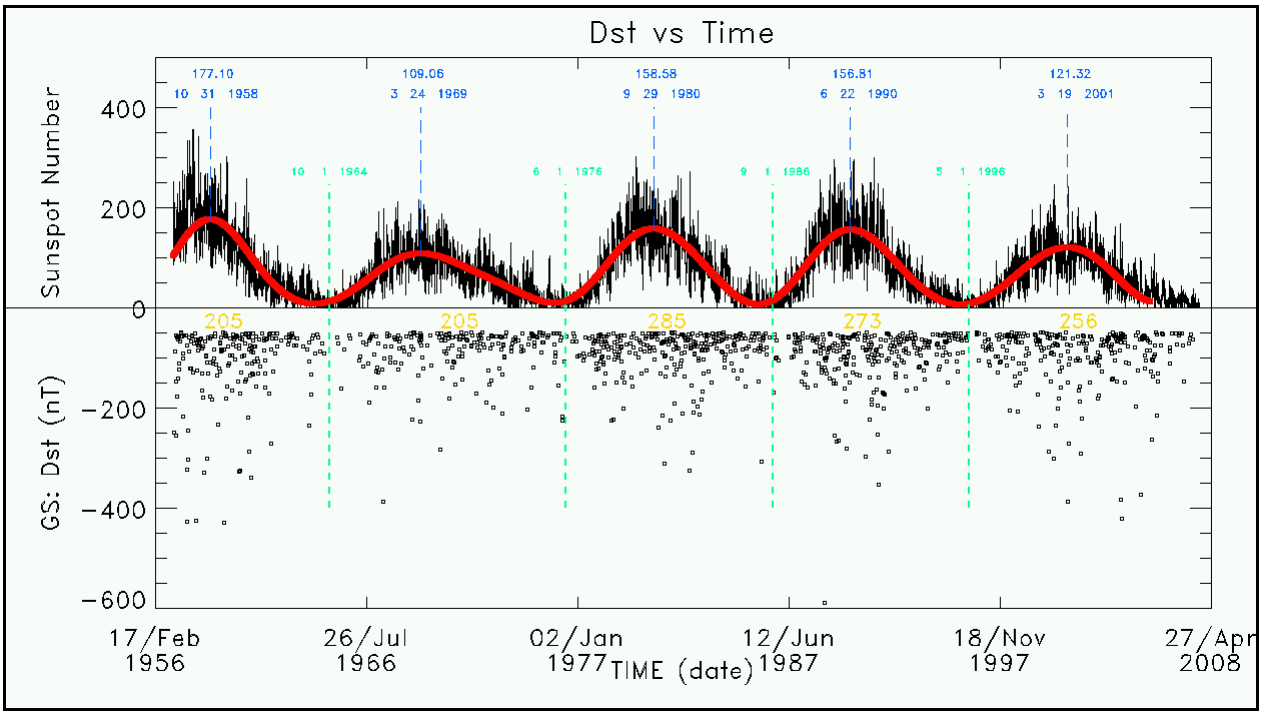

Figure 5: Distribution of GS vs. time. Black dots correspond to Dst minimum of the GS. Solar maximum and minimum activity are delineated (green and blue lines respectively, dates indicated), corresponding to solar cycles 19 (incomplete), 20, 21, 22 and 23. Sunspot number is plotted on the black curve with superimposed smoothed curve in red. The number of storms is outlined for each of the solar cycles (orange).

A direct result of this distribution is that the time interval between storms, for SC 21 and SC 22, is shorter than for the less severe cycles. In order to confirm that SSN is the best parameter to represent solar cycle activity statistics, the analysis was previously performed with the f10.7 cm index[7], which did not give such a good agreement as SSN (Fig. 6). There is a logarithmic relationship between number of storms per month in a solar cycle vs. sunspot number that can give the first and simplest prediction of the overall number of geomagnetic storms expected for the next solar cycle, if the sunspot maximum can be forecasted.

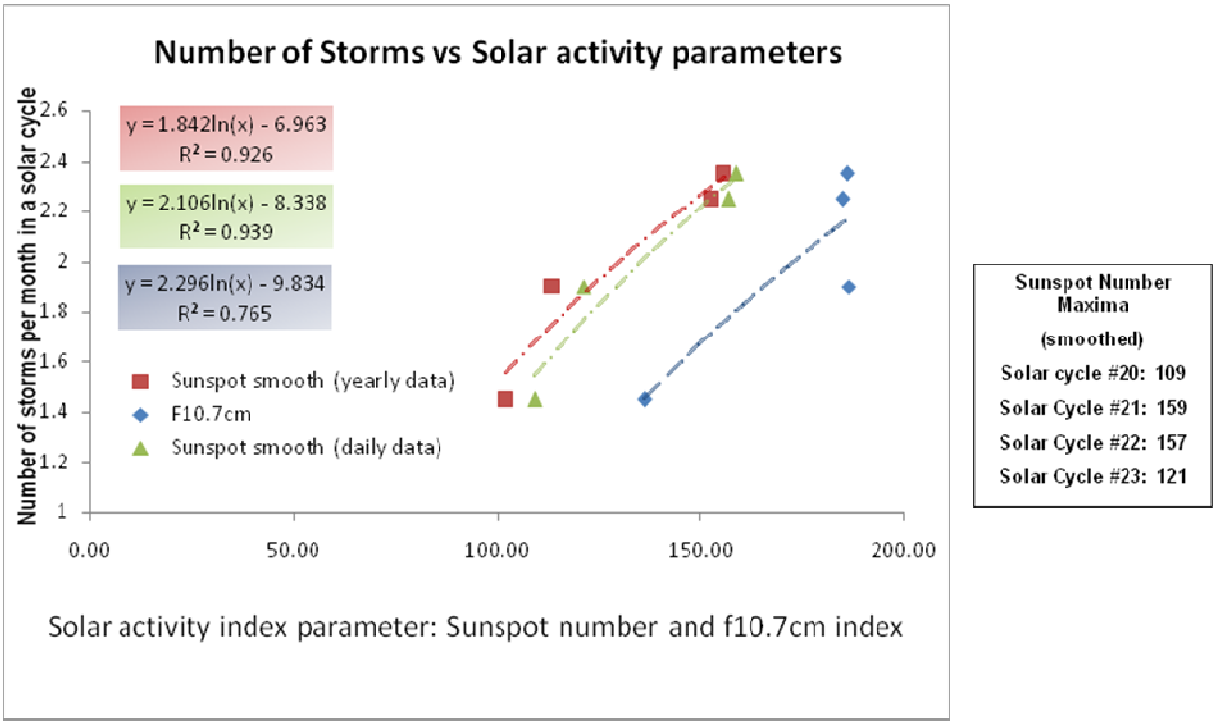

Figure 6: Number of storms per month as a function of solar activity index parameters: Sunspot number (yearly data and daily data) and f10.7cm index. The total number of storms in a cycle correlates directly to the severity of the solar cycle: For solar cycles with higher SSN maxima, SC 21 and SC 22,the total number of storms is higher than for SC 20 and SC 23 with lower maxima.

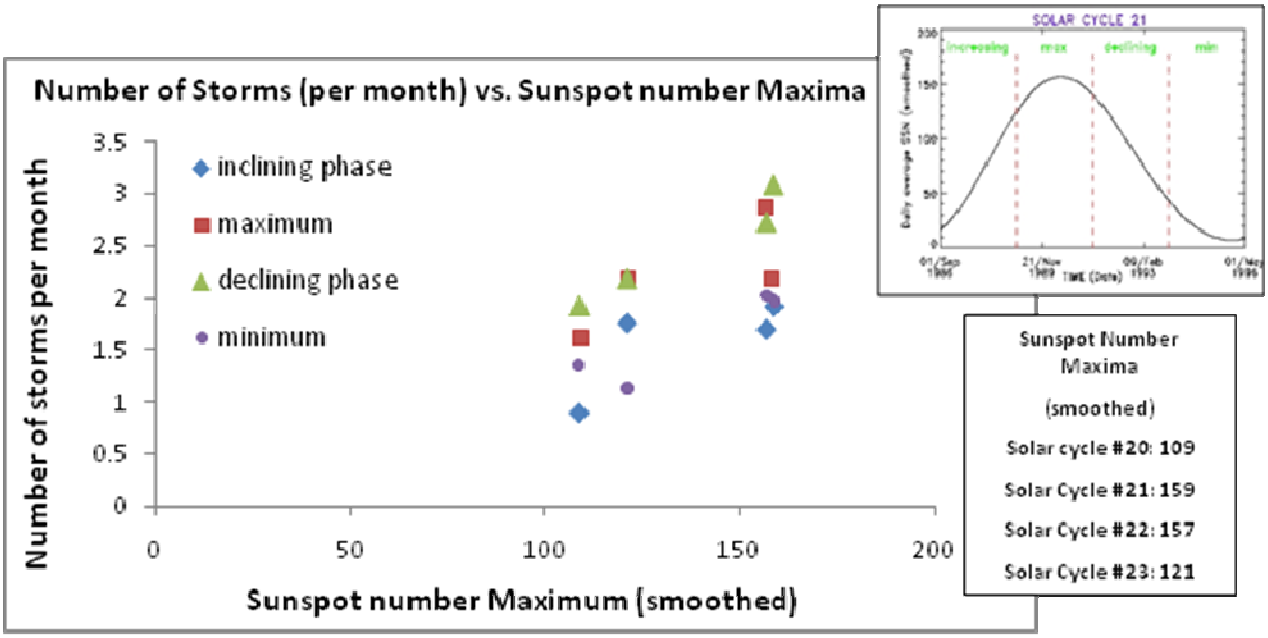

Figure 7: Number of storms per month as a function of solar phase and solar cycle severity

Furthermore, the solar cycles were arbitrarily divided into four equal intervals of time corresponding to the different phases within the solar cycle (increasing, maximum, declining, and minimum) to extend the comparison to the phases for all the cycles, which statistically confirmed the intuitive idea that declining phase and solar maximum are indeed the most active periods (Fig. 7). Moreover, severe solar cycles result in

higher number of storms per month for the declining phase than those with lower sunspot maximum, increasing the probability of having a storm after another one, for a given time interval. The relationship also extends to the other phases within the solar cycle.

An extensive study of different phases of the solar cycles revealed a difference in probability depending on the severity of the solar cycle: The probability of having a severe GS after a short time interval is larger for higher SSN maximum cycles during the declining phase (Fig. 8), noticeable for all phases and all cycles, and it can be used to predict GS occurrences for the new solar cycle if the sunspot number maximum is suspected.

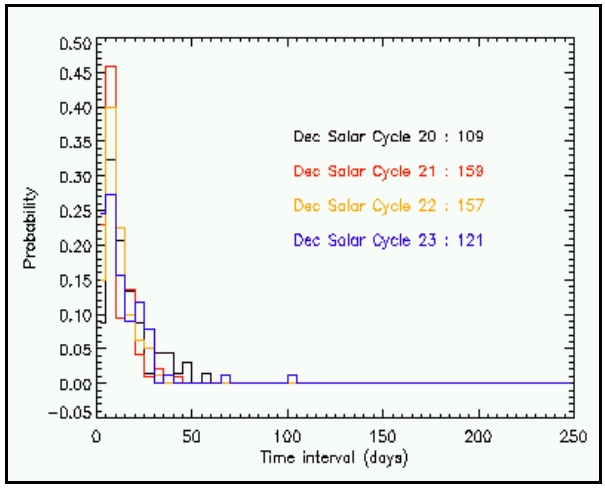

Figure 8 (a): Probability of having a GS after another for a given time interval.

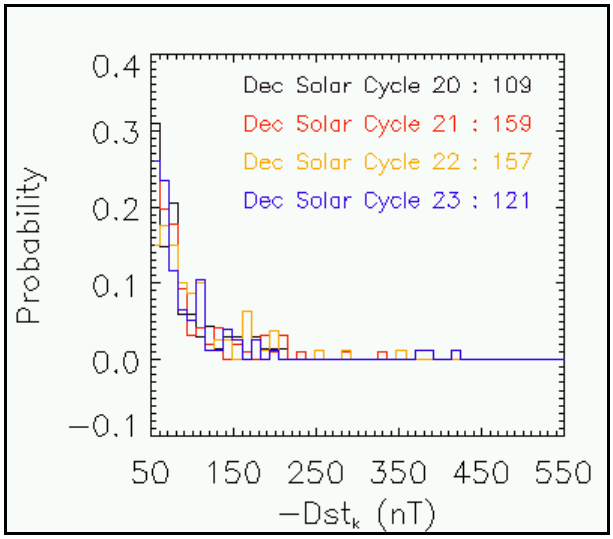

Figure 8 (b): Probability of having a GS of a given Dst_k after another GS of any magnitude, for the declining phase of the different solar cycles.

5. PRELIMINARY RESULTS

In order to establish a relationship between storm characteristics and the resulting electron flux enhancement, flux data from different sources were analyzed, to determine decay time T, steady state for quite times ϕ_{st}, and maximum flux reached after a storm of certain magnitude ϕ_0.

Decay time of fluxes, after storm time, have been evaluated as a function of energy and position [Benck et al, 2007] [8] for the DEMETER[9] data set, and was found to be directly proportional, with increasing L, for lower energies and inversely proportional for higher energies. Low energy electrons decay time T is higher at low L and it is lower for high energy electrons at these L values.

The IDP detector, carried by DEMETER, was cross-validated with the ICARE detector carried by SAC-C [10]. The SAC-C data[11] was used to recover the steady state ϕ_{st}, during a period of more than 100 days with no magnetic storms, in 2004, since the DEMETER satellite was launched after that period.

A plot of the steady state flux vs. L for different energies (Fig. 9) shows that the steady state is almost zero for L values lower than 4; for higher values of L, the steady state increases for decreasing energies. It must be stressed that cross-calibration of instruments should use such kind of steady state fluxes since they are not likely to be modified by storm-time events.

Using the SAC-C flux data, we have identified 13 GS events in 2001-2005 for which the magnitude of the flux enhancement difference goes in hand with the magnitude of the storms, for electrons between 0.521 and 0.968 MeV for L > 2.5 and B >0.22 nT. The analysis was performed for a discriminating L binning of an increment of 0.2 L, for all energies. The storms were separated into three groups, corresponding to isolated CME storms, isolated CIR storms, and mixed non isolated storms. An linear correlation between GS amplitude and flux enhancement difference ΔF reached after the storm was found for the isolated storms (Fig. 10), giving higher flux differences for a given GS amplitude for CIR storms. Since the recovery time is longer for these type of storms, there is more time for flux enhancement, reaching a higher maximum, and therefore, a higher flux difference.

In a first attempt to measure δ, the time interval between Dst_{prev} and maximum flux, as a function of L, the distribution seems to be linear for all thirteen isolated storms, but random for all other storms. More analysis is needed, such as discriminating the type of storm, time for the storm to recover, etc.

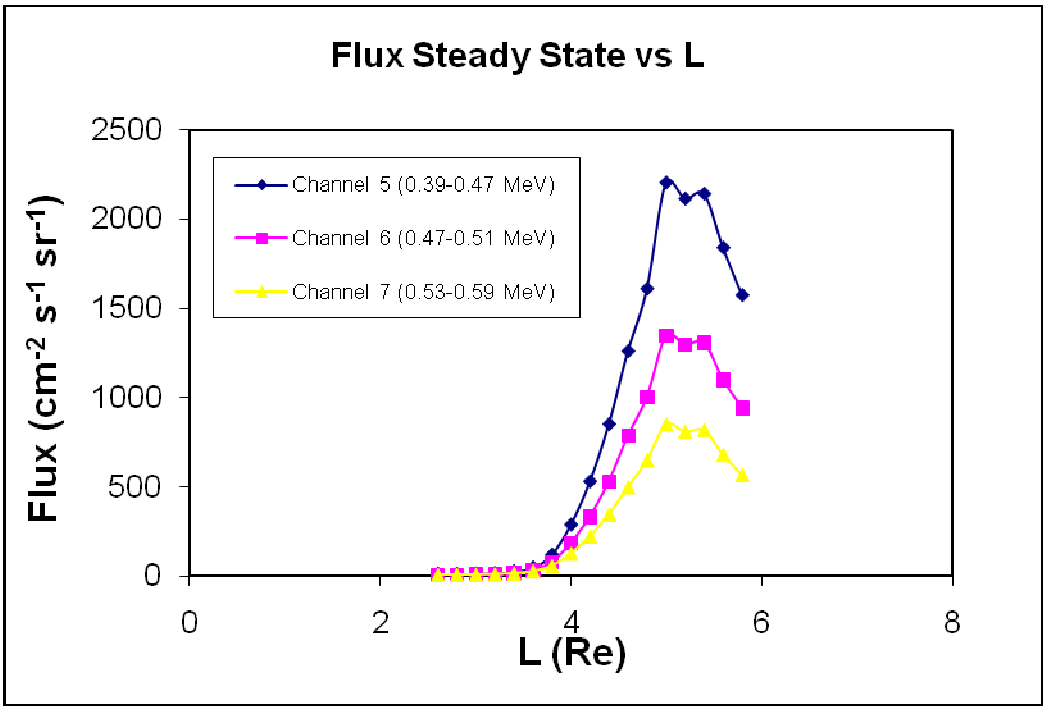

Figure 9: Electron flux as a function of L, corresponding to steady state (SAC-C).

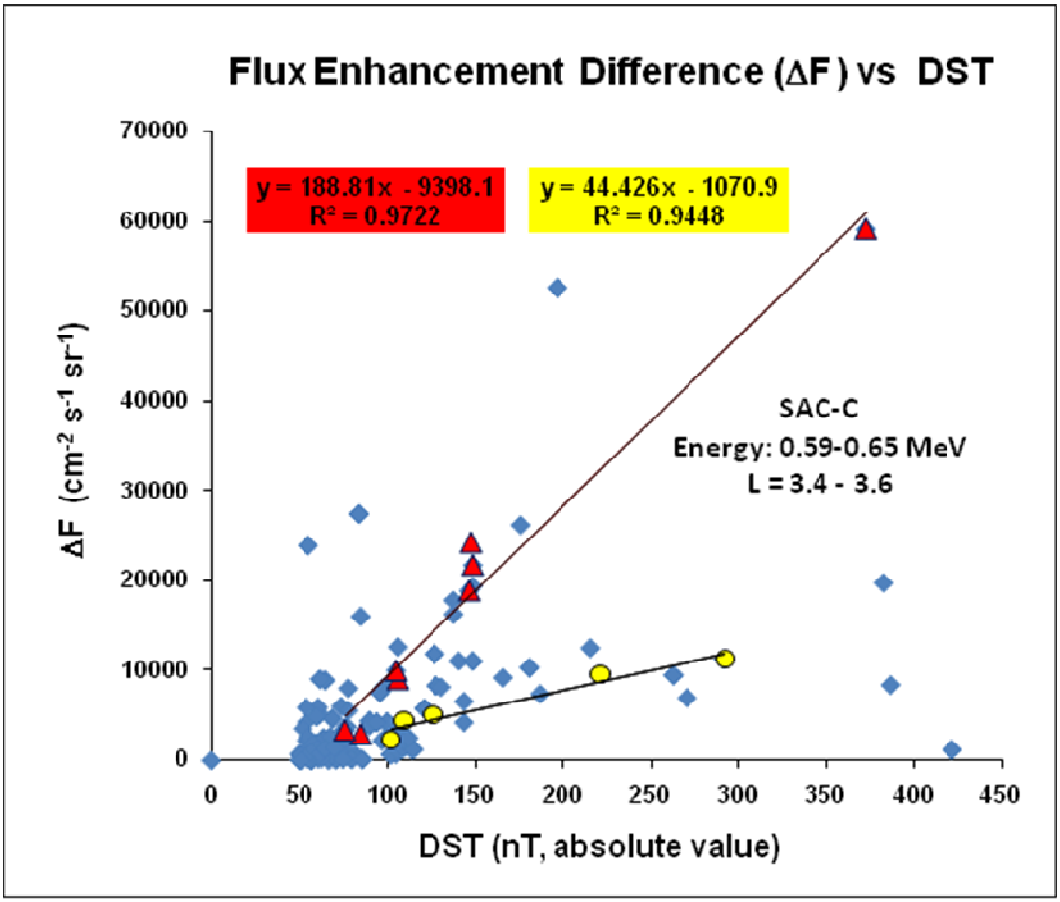

Figure 10: Resultant flux enhancement difference as a function of storm severity, corresponding to isolated CME's (yellow), CIR's (red), and mixed non isolated storms (blue)

6. CONCLUSIONS

In these preliminary studies, we have introduced the statistical dynamic model based on physical phenomena that were parameterized using observables like Dst, the maximum flux after the recovery phase of the storm, the decay time, etc . We have successfully evaluated almost all parameters ($\Delta\phi_{res,}$ $\phi_{0,}$ $\phi_{st,}$ *T)* needed to derive the statistical model and test it.

The correlation between flux enhancement difference and magnetic storm strength was successfully established, and the steady state flux was found for different positions and energies. The time interval between storms follows a poissonnian distribution, and present a nice agreement with the smoothed sunspot number, that would allowed to predict fluxes for different phases within the solar cycle. More data is needed for extended periods of time, for previous cycles to complete analysis, as well as other regions, since only the LEO orbit has been explored in this study. The team at CSR will continue to provide efforts to finalize this study that would allow to predict flux dynamics for different regions and different energies.

Acknowledgements
CSR would like to thank CNES/DCT/AQ/EC Section, ONERA/DESP and CONAE, for the SAC-C data. Laura Mazzino would like to thank Dr. Joseph Lemaire and Dr. Viviane Pierrard for their invaluable help discussing the main topics presented here.

[1]Xapsos, M.A., S.L. Huston, J.L. Barth (2002), Probabilistic model for low-altitude trapped-proton fluxes, *IEEE Transactions on nuclear science*, vol. 49. No.6 Dec. 2002
[2]Gussenhoven, M.S., E.G. Mullen, D.H. Brautigam (1996), Phillips laboratory space physics division radiation models, *Geophysical Monograph* 97, p. 93
[3]McIlwain, C.E. (1996), Processes acting upon outer zone electrons, *Geophysical Monograph* 97, p. 15
[4] Kataoka, R and Y. Miyoshi (2006), Flux enhancement of radiation belt electrons during geomagnetic storms driven by coronal mass ejections and corotating interaction regions, *Space Weather,* 4, S09004, doi:10.1029/2005SW000211.
[5]Data Analysis Center for Geomagnetism and Space Magnetism Graduate School of Science, Kyoto University (http://swdxww.kugi.kugi.kyoto_u.ac.jp/index.html)
[6]SIDC Solar Influences Data Analysis Center (http://sidc.oma.be/sunspot-data/)
[7]Dominion Radio Astrophysical Observatory (http://www.drao-ofr.hia-iha.nrc-cnrc.gc.ca/icarus/www/archive.html)
[8]Benck, S., M. Cyamukungu, D. Bertrand, J. Cabrera (2007), Study of correlations between waves and particle fluxes measured on board the DEMETER satellite. *Advances in Space Research (ASR)* Last revision in February, 2008.
[9]Cussac, T., M. Clair, P. Ultre-Guerard, F. Buisson, G. Lassalle-Balier, M. Ledu, C. Elisabelar, X. Passot, and N. Rey (2006), The Demeter microsatellite and ground segment, *Planetary and Space Science,* vol. 54, issue 5, April 2006, pages 413-427, doi:10.1016/j.pss.2005.10.013
[10]Colomb, F.R., C. Alonso, I. Nollman, (2004) SAC-C mission, and example of international cooperation *Advances in Space Research (ASR)*, vol. 34, issue 10, Pages 2194-2199, doi:10.1016/j.asr.2003.10.039
[11]SAC-C Data: Courtesy of CNES/DCT/AQ/EC Section, ONERA/DESP and CONAE